Elisa Magnanelli*, Øivind Wilhelmsen, Mario Acquarone, Lars P. Folkow and Signe Kjelstrup

The Nasal Geometry of the Reindeer Gives Energy-Efficient Respiration

DOI 10.1515/jnet-2016-0038
Received April 30, 2016; revised July 4, 2016; accepted June 17, 2016

Abstract: Reindeer in the arctic region live under very harsh conditions and may face temperatures below 233 K. Therefore, efficient conservation of body heat and water is important for their survival. Alongside their insulating fur, the reindeer nasal mechanism for heat and mass exchange during respiration plays a fundamental role. We present a dynamic model to describe the heat and mass transport that takes place inside the reindeer nose, where we account for the complicated geometrical structure of the subsystems that are part of the nose. The model correctly captures the trend in experimental data for the temperature, heat and water recovery in the reindeer nose during respiration. As a reference case, we model a nose with a simple cylindrical-like geometry, where the total volume and contact area are the same as those determined in the reindeer nose. A comparison of the reindeer nose with the reference case shows that the nose geometry has a large influence on the velocity, temperature and water content of the air inside the nose. For all investigated cases, we find that the total entropy production during a breathing cycle is lower for the reindeer nose than for the reference case. The same trend is observed for the total energy consumption. The reduction in the total entropy production caused by the complicated geometry is higher (up to -20 %) at more extreme ambient conditions, when energy efficiency is presumably more important for the maintenance of energy balance in the animal. In the literature, a hypothesis has been proposed, which states that the most energy-efficient design of a system is characterized by equipartition of the entropy production. In agreement with this hypothesis, we find that the local entropy production during a breathing cycle is significantly more uniform for the reindeer nose than for the reference case. This suggests that natural selection has favored designs that give uniform entropy production when energy efficiency is an issue. Animals living in the harsh arctic climate, such as the reindeer, can therefore serve as inspiration for a novel industrial design with increased efficiency.

Keywords: thermodynamics, *Rangifer tarandus*, transport, nose, breathing, reindeer, energy efficiency, entropy production

1 Introduction

Reindeer (*Rangifer tarandus*) have a distribution that extends into the arctic and may, hence, experience harsh climatic conditions. In the winter, they might face temperatures below 233 K, which is very energetically demanding for the animal [1], and which is further aggravated by the fact that water is available only in the form of snow. Under these conditions, reindeer need to minimize heat and water losses. During the arctic winter, they are protected against cold by fur with outstanding insulating properties [2, 3]. Alongside this protection, they possess efficient thermoregulatory mechanisms that help them minimize heat loss to the surroundings [4–6]. In this context, the reindeer nasal heat and mass exchange mechanisms play an

***Corresponding author: Elisa Magnanelli,** Department of Chemistry, NTNU – Norwegian University of Science and Technology, N-7491 Trondheim, Norway, E-mail: elisa.magnanelli@ntnu.no
Øivind Wilhelmsen, SINTEF Energy Research, N-7465 Trondheim, Norway; Department of Electrical Engineering and Renewable Energy, NTNU, N-7491 Trondheim, Norway
Mario Acquarone, Lars P. Folkow, Department of Arctic and Marine Biology, University of Tromsø – The Arctic University of Norway, N-9037 Tromsø, Norway
Signe Kjelstrup, Department of Chemistry, NTNU – Norwegian University of Science and Technology, N-7491 Trondheim, Norway

important role in minimizing body heat and water which are lost upon respiration [6]. Heat and moisture that are added to the ambient air from the mucosal linings of the nasal cavity during inhalation are partially recovered upon exhalation, when the warm and moist air from the lungs meets the cooler mucosal linings on its way out of the animal. Thus, the saving mode is based on the recovery of heat from the exhaled air and on the subsequent condensation of water. Previous studies have shown how the heat and water recovery capacity in animals is generally higher than in humans [6, 7]. In particular, reindeer have evolved very complex anatomical structures in the nasal cavity (see Figure 1), called nasal turbinates [8–11], which enable them to recover large amounts of the heat and water from the exhaled air stream by giving it off to the mucosa lining that has been cooled down upon inhalation [6]. Given the complexity of the nasal structure, it is natural to ask about which role the complicated nose geometry plays in recovering heat and water during respiration.

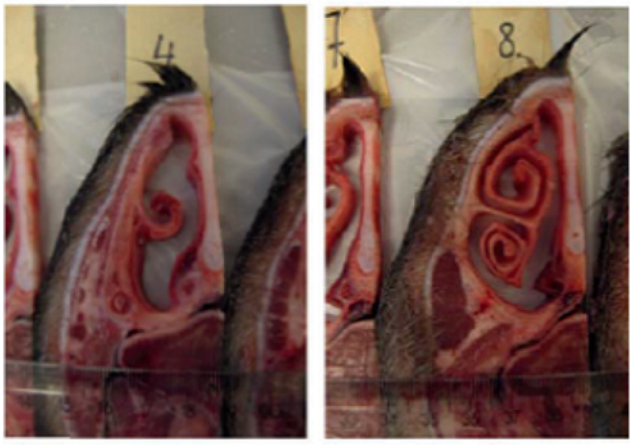

(a) (b)

Figure 1: Cross sections of a reindeer nose at 6 cm (a) and 10 cm (b) into the nose.

Two cross sections of the reindeer nose are shown in Figure 1, where scroll-type turbinate structures are sectioned perpendicularly to the axis of the nose. The mucosal lining of walls and turbinates of the nasal cavity is covered by a thin layer of mucus that keeps the lining wet. During respiration, water and heat are exchanged across this layer. The convolutions are less complex toward the nostrils (Figure 1(a)) than in the more proximal section (Figure 1(b)). Thus, there is an increase in convolution complexity toward the middle of the turbinate scroll.

The hypothesis to be investigated in this work can be formulated as follows: is the nose geometry leading to a gradient in air-flow velocities and contact-area profiles inside the nose which are beneficial for the animal in a thermodynamic sense? Does this structure lead to more efficient heat and water recovery than a simple nose structure? In order to answer these questions, we will examine a model that mimics the real structure of the reindeer nose (Figure 1) and compare it to a reference case, where we model a nose with uniform geometrical properties but with the same total contact areas and volume as the reindeer nose. We shall address the questions by using non-equilibrium thermodynamics, and we discuss the issue of optimal design from an evolutionary perspective. With non-equilibrium thermodynamics, we can objectively assess whether the complicated geometry of the reindeer nose is advantageous with respect to the thermodynamic efficiency. The overall idea is that further knowledge on natural systems can inspire the engineering of, for instance, new and more efficient heat and water exchangers. This is of relevance for the treatment of the exhausted air from ventilation systems of buildings. Similar ideas have already led to the proposal of a new improved fuel cell design [12, 13].

It is known from thermodynamic optimization studies of industrial equipment [14–16] that processes with high-energy efficiency are characterized by a uniform distribution of the local entropy production. In

agreement with these, we will show that the geometry of the reindeer nose gives a significantly reduced total entropy production as well as a more uniform local entropy production than the reference case. Moreover, the relative improvement in energy efficiency due to the complicated geometry of the reindeer nose is larger at lower ambient temperatures, when the energy efficiency of the animal is more important. This shows that the nose geometry is likely of evolutionary advantage to the animal for surviving in the harsh arctic climate and that the geometry is particularly advantageous at very low ambient temperatures.

Several models are available in literature to describe heat and water exchange in the human nasal cavity, and we refer to Ref. [17]. for an accurate review. In most of these works, the air temperature and humidity were the only parameters that were modeled, and the boundary conditions at the air–wall interface for temperature and water vapor concentration were assumed to be constant [18–20]. This is a reasonable assumption for humans at ambient temperature around 293 K, but not for reindeer, where the inhaled air can reach temperatures of 233 K or less. Attempts to model the respiratory heat and water transfer in animals have dealt with the steady state only (e. g. Ref. [21]). This work presents the first model that properly includes all relevant subsystems that concur to the dynamic energy and mass balances in the nose.

2 The system

The nose of a reindeer is a very complex system (Figure 1). The nasal cavities contain double scroll-like structures composed of cartilage covered by a thin, richly vascularized mucosal lining which also covers the walls of the cavity [10, 11, 22]. Outermost, a thin layer of mucus keeps the lining wet. The mucosal blood vessels form an intricate network of frequently anastomosing veins and arteries that run in the longitudinal direction of the nasal cavities [10, 22]. In order to model the nose, we need to simplify the nature of the system. The model we consider is composed of five interconnected subsystems as depicted in Figure 2, which exchange mass and heat:

– The nasal cavity is filled with air that runs from the ambient (distal extremity of the nose) to the lungs (proximal extremity) during inhalation and in the opposite direction during exhalation. The air is considered to be a mixture of gases with a variable percentage of humidity. State variables are cross-section averaged. The air flow in and out of the nose is caused by variation in pulmonary pressure due to the expansion and contraction of the thoracic cavity. However, since the maximum difference between the ambient pressure and the pulmonary pressure is typically lower than 300 Pa (0.3 % of the ambient pressure) during quiet breathing, we will assume that the total average pressure is

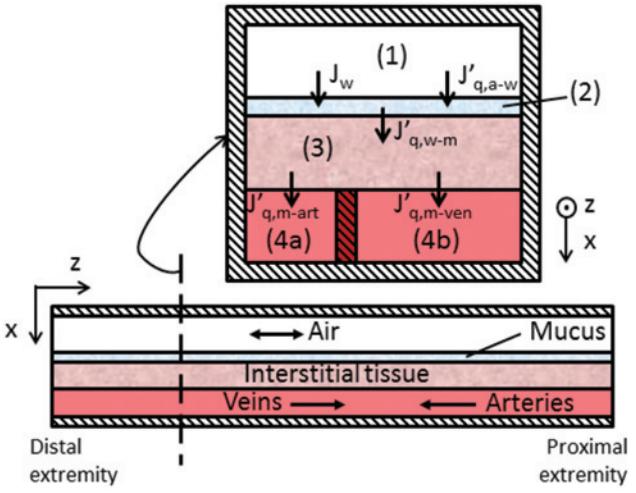

Figure 2: Illustrative representation of how the different parts of the nose interact. For the explanation of the notation used in the figure, we refer to Section 3.

constant along the nasal cavity and equal to the ambient pressure. As a further simplification, we assume that the dry air has constant molar composition (79 % nitrogen and 21 % oxygen), neglecting the variation in the content of oxygen and carbon dioxide during the different phases of the breathing cycle, as well as the presence of small amounts of other gases. During inhalation, the air enters the distal extremity of the nose at ambient conditions of temperature and humidity. During exhalation, we assume that saturated air at the reindeer deep body temperature leaves the lungs and enters the proximal extremity of the nose.

- The mucus layer provides water for humidification of the air, preventing the tissues underneath from dehydration. During inhalation, cold and relatively dry ambient air enters the nose. The inhaled air is warmed up and humidified by the mucus layer, as it flows through the nasal cavity. During exhalation, the saturated warm air coming from the lungs undergoes the opposite process. Not all the water is recovered during exhalation, and the lost water is replaced by mucus-generating tissues (serous glands).
- The interstitial tissues act as a capacity for storage of energy and delay the heat exchange process. The interstitial tissues are abundantly irrigated by blood, and their density is assumed to be constant.
- Arteries and veins run through the interstitial tissues. The pressure and the density of the blood inside them are considered constant. In general, the blood flow can be regulated for thermoregulatory purposes. However, under a specific thermal condition, the flow can be assumed to be constant in time and space. Therefore, the velocity of the blood in arteries and veins varies depending on the vessel cross sections only. In general, veins and arteries have the ability to contract and distend to regulate blood flow; therefore, their cross section can vary in time. However, since we have no information about this dependency, we will consider all the geometrical variables (cross-sectional areas and perimeters) to be functions of the spatial coordinates only. According to Casado Barroso [10], the total cross section of venous vessels is six to ten times larger than the one of arteries.

2.1 Investigated cases

We have analyzed and compared the mass and heat exchanged in two systems with different geometries:

System A – reindeer nose model: Cross-sectional perimeters and areas of the subsystems are taken from anatomical studies [10], where the geometry of a reindeer nose has accurately been determined. The geometry of all subsystems varies along the z-coordinate. We report the geometry of the nasal cavity in Figure 3 as an example. The thick lines represent the variation of the cross-sectional perimeter (solid line)

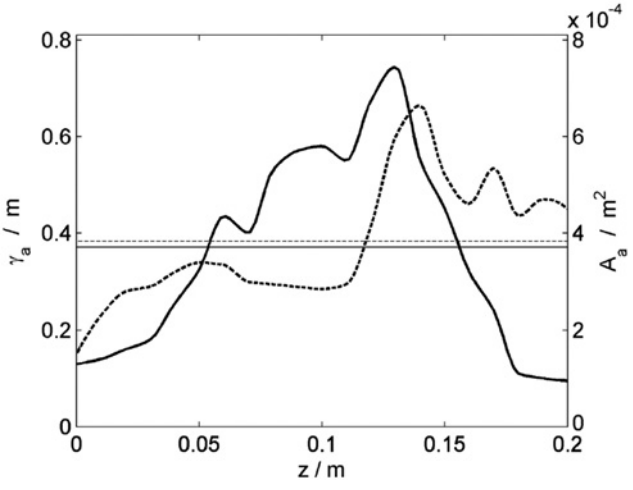

Figure 3: Cross-sectional perimeter (solid line) and area (dashed line) of the nasal cavity, from the distal to proximal extremity of the nose. The thick lines are derived from data in Ref. [10] and used in System A; the thin lines represent the averaged cross-sectional perimeter and area used in System B.

and of the cross-sectional area (dashed line) of the nasal cavity, from the distal extremity of the nose to the proximal one. Similar geometrical parameters are used also for the other subsystems.

System B – cylindrical-like heat and mass exchanger: Cross-sectional perimeters and areas of the subsystems are constant along the z-coordinate. In order to make System B comparable with System A, the averaged cross-sectional areas and perimeters are such that the total volume and the total contact area of the subsystems are the same in the two cases. The thin lines in Figure 3 represent the constant cross-sectional perimeter (solid line) and the constant cross-sectional area (dashed line) of the nasal cavity for System B.

3 Theoretical formulation

In Sections 3.1 and 3.2, we state the mass and energy balances used to describe the evolution of the thermodynamic properties in every subsystem as a function of time and space. Section 3.3 deals with transport across the surface between two neighboring systems (x-direction). We address the description of transport using the framework of non-equilibrium thermodynamics. Section 3.4 deals with the calculation of the heat and water recovery, while Section 3.5 describes the calculation of the entropy production.

3.1 Mass balances

As mentioned in Section 2, we use a particular form of the mass and energy balance [23], where the thermodynamic properties are integral averaged over the cross section of each system. Humid air flows in the nasal cavity, and the content of water varies in time and space. Therefore, two mass balances are needed to describe this subsystem. We use the subscripts a, dry and w,a to refer to the thermodynamic variables of the humid air, of the dry air and of water content in the air respectively. For simplicity, we establish a mass balance for the dry air and one for the water content in the air:

$$\frac{\partial\left(A_a \rho_{dry}\right)}{\partial t} = -\frac{\partial F_{dry}}{\partial z} \tag{1}$$

$$\frac{\partial\left(A_a \rho_{w,a}\right)}{\partial t} = -\frac{\partial F_{w,a}}{\partial z} - J_w \gamma_a \tag{2}$$

where t is the time coordinate, ρ indicates the density, F represents the mass flow rate, and A and γ are the area and perimeter of the cross section of the considered subsystem, at the z-position. Finally, J_w is the mass flux of condensing or evaporating water, which is exchanged between the air stream and the mucus layer. An expression for it is presented in Section 3.3.

A water flux is continuously present between the mucus layer and the air stream. The mucus layer is also fed by mucus generating tissues, which provide the water that is not recovered during exhalation. This, together with the fact that the amount of water that is evaporated and condensed over the breathing cycle is small in comparison to the amount of mucus, leads us to the assumption of constant mucus layer thickness, d_m. Moreover, since the mucus layer thickness is very small in comparison to the perimeter of the system, we assume that the perimeter of the interface with the air stream, γ_a, and the perimeter of the interface with the interstitial tissue, γ_m, are equal to each other, and that $A_m = \gamma_a d_m = \gamma_m d_m$. We use the subscript m to denote the thermodynamic variables of the mucus layer. With the above assumptions, the mass balance for the mucus layer becomes

$$\frac{\partial(A_m \rho_m)}{\partial t} = J_w \gamma_a + J_m \gamma_m \tag{3}$$

where J_m is the mucus flux that is produced by the mucus-generating tissues. The density of the mucus is assumed to be constant. Because of the assumptions made, eq. (3) equals 0.

The subscript *it* is used to describe the thermodynamic variables of the interstitial tissues. In the interstitial tissues, no mass transport takes place. Therefore, the mass balance reduces to

$$\frac{\partial(A_{it}\,\rho_{it})}{\partial t} = 0 \tag{4}$$

Since the interstitial tissues are strongly irrigated by blood, we assume ρ_{it} to be equal to the density of the blood, ρ_b, and constant.

We use the subscripts *art* and *ven* to refer to the thermodynamic variables of the arterial and vein systems, respectively. Since we consider the vascular system to be impermeable, no mass flux is exchanged between arteries, veins and the interstitial tissues:

$$\frac{\partial(A_{art}\,\rho_b)}{\partial t} = -\frac{\partial F_{art}}{\partial z} \tag{5}$$

$$\frac{\partial(A_{ven}\,\rho_b)}{\partial t} = -\frac{\partial F_{ven}}{\partial z} \tag{6}$$

The blood flow enters the system via the arterial vessels at the proximal extremity of the nose and flows through the system along the z-direction. At the distal extremity of the nose, arteries communicate with veins. From there, the blood crosses the nose again into the vein vessels, which run in a counter-current fashion with respect to the arterial system, to exit the system at the proximal extremity of the nose [22]. Thus, the flow of blood in arteries and veins is the same but with opposite direction, $F_{art} = -F_{ven}$. Since we consider the blood density to be constant, eqs. (5) and (6) are equal to 0.

3.2 Energy balances

We use the area averaged form of the balance equations also for the energy [23]:

$$A_a\,\rho_a\,c_{p,a}\frac{\partial T_a}{\partial t} = -F_a\,c_{p,a}\frac{\partial T_a}{\partial z} - J'_{q,a-m}\,\gamma_a + J_w(h_a - h_{w,a})\gamma_a - A_a\,\rho_a\sum_i h_i\frac{\partial w_i}{\partial t} - F_a\sum_i h_i\frac{\partial w_i}{\partial z} \tag{7}$$

$$A_m\,\rho_m\,c_{p,m}\frac{\partial T_m}{\partial t} = (J_w\,h_{w,a} - J_m\,h_{w,m})\gamma_m + \left(J'_{q,a-m} - J'_{q,m-it}\right)\gamma_m \tag{8}$$

$$A_{it}\,\rho_{it}\,c_{p,b}\frac{\partial T_{it}}{\partial t} = J'_{q,m-it}\,\gamma_m - J'_{q,it-art}\,\gamma_{art} - J'_{q,it-ven}\,\gamma_{ven} \tag{9}$$

$$A_{art}\,\rho_b\,c_{p,b}\frac{\partial T_{art}}{\partial t} = -F_{art}\frac{\partial T_{art}}{\partial z} + J'_{q,it-art}\,\gamma_{art} \tag{10}$$

$$A_{ven}\,\rho_b\,c_{p,b}\frac{\partial T_{ven}}{\partial t} = -F_{ven}\frac{\partial T_{ven}}{\partial z} + J'_{q,it-ven}\,\gamma_{ven} \tag{11}$$

where T is the temperature, c_p is the specific heat capacity, h is the mass enthalpy, and w_i is the mass fraction of the component i in air. The mass density of the humid air equals the sum of the densities of the dry air and of the water content in the air ($\rho_a = \rho_{dry} + \rho_{w,a}$). A similar relation applies to the air mass flow ($F_a = F_{dry} + F_{w,a}$). The dry air is assumed to contain just oxygen and nitrogen, in fixed proportion. The heat capacity of the interstitial tissues is assumed to be equal to that of blood. Here, $J'_{q,a-m}$, $J'_{q,m-it}$, $J'_{q,it-art}$ and $J'_{q,it-ven}$ are the measurable heat fluxes that are exchanged between air and mucus layer, mucus layer and interstitial tissues, interstitial tissues and arteries, and interstitial tissues and veins. Section 3.3 presents an expression for them.

3.3 Transport across the subsystems' interfaces

In order to describe the transport between two neighboring subsystems i and j, it is necessary to consider both the contribution to the heat and mass transport coefficients due to the interface, R_{i-j}^{interf}, and the contribution associated with convection, R_i^{conv} and R_j^{conv} (for subsystems where mass flow is present). These coefficients can be combined as resistances in series, in analogy with electrical circuits, to obtain an overall transport coefficient:

$$R_{i-j} = R_i^{conv} + R_{i-j}^{interf} + R_j^{conv} \tag{12}$$

At the interface between the humid air and the mucus layer, both heat and mass are exchanged. The coupling between heat and mass transport has been found to be important at a liquid vapor interface [15, 24, 25]. The use of non-equilibrium thermodynamics allows one to take this coupling consistently into account. The heat and mass transport between the humid air and the mucus layer can be described by the equations:

$$\frac{1}{T_m} - \frac{1}{T_a} = R_{qq,\,a-m} J'_{q,\,a-m} + R_{q\mu,\,a-m} J_w \tag{13}$$

$$-\left(\frac{\mu_{w,m}}{T_m} - \frac{\mu_{w,a}}{T_a}\right) + h_{w,a}\left(\frac{1}{T_m} - \frac{1}{T_a}\right) = R_{\mu q,\,a-m} J'_{q,\,a-m} + R_{\mu\mu,\,a-m} J_w \tag{14}$$

where μ indicates the chemical potential. Here, $R_{ii,\,a-m}$ and $R_{ij,\,a-m}$ are respectively the main and coupling transport coefficients between the two subsystems, where $i, j \in \{q, \mu\}$. Since we neglect the convection contribution to the coupling coefficients, we find that $R_{ij,\,a-m} = R_{ij,\,a-m}^{interf}$. The Onsager reciprocal relation relates the coupling transport coefficients, $R_{ij,\,a-m}^{interf} = R_{ji,\,a-m}^{interf}$, reducing the number of independent coefficients to 3 [26, 27]. According to non-equilibrium thermodynamics, the transport coefficients of a planar surface in a single-component fluid are functions of the surface temperature only [15]. For water at temperature below 560 K, it has been found that the temperature of the surface equals a good accuracy the temperature of the liquid phase, and the interface transport coefficients of water have been tabulated in Ref. [28].

The convective contribution to heat transport depends on the characteristics of the flow of the fluid, and it can be calculated from the convective heat transport coefficient of the system, h:

$$R_{qq,\,a-m}^{conv} = \frac{1}{T_a^2 h} \tag{15}$$

The convective transport coefficient can be calculated from the Nusselt number:

$$\mathrm{Nu} = \frac{h D_a}{\lambda_a} \tag{16}$$

where $D = 4\gamma/A$ is the hydraulic diameter of a cross section, and λ is the thermal conductivity. Empiric relations exist for the determination of the Nusselt number according to the characteristics of the flow. The literature about air-flow conditions in human nasal cavity has divided opinions on the laminar or turbulent nature of the air flow [29]. Due to the much higher complexity of the the reindeer nose structure in comparison to the human one, we assume the air flow to be in the turbulent regime. The Nusselt number in turbulent flow is related to the friction factor through the Chilton–Colburn analogy [30]:

$$\mathrm{Nu} = 0.125 f\, Re\, Pr^{1/3} \tag{17}$$

where f is the friction factor, Re is the Reynolds number, and Pr is the Prandtl number. An expression for the friction coefficient in the human nasal cavity for similar respiratory minute volumes (V_{min}) is available [31]:

$$f = \frac{47.78}{Re}\left(1 + 0.127\, Re^{0.489}\right) \tag{18}$$

The convective contribution to mass transport can be calculated from the convective mass transport coefficient, k_c:

$$R^{conv}_{\mu\mu,\,a-m} = \frac{1}{T_a\,k_c}\frac{d\mu_{w,\,a}}{\mathrm{d}\rho_{w,\,a}} \tag{19}$$

The convective mass transport coefficient can be calculated from the Sherwood number:

$$\mathrm{Sh} = \frac{k_c\,D_a}{D_{w,\,a}} \tag{20}$$

where $D_{w,\,a}$ is the mass diffusivity of water in air. The Sherwood number in the turbulent regime inside pipes can be calculated as

$$\mathrm{Sh} = 0.023\,Re^{0.8}\,Sc^{1/3} \tag{21}$$

where Sc is the Schmidt number.

Only heat is exchanged between the other subsystems:

$$\frac{1}{T_j} - \frac{1}{T_i} = R_{q,\,i-j}\,J'_{q,\,i-j} \tag{22}$$

where $R_{q,\,i-j} = R^{conv}_{q,\,i} + R^{interf}_{q,\,i-j} + R^{conv}_{q,\,j}$ is the thermal transport coefficient between the i and j neighboring subsystems. Since no information about the resistance to heat transport of these surfaces is available, we can estimate $R^{interf}_{q,\,i-j}$ by multiplying the heat transport coefficient in the rate determining phase next to the interface (either $R_{q,\,i}$ or $R_{q,\,j}$) with the interface thickness. The heat transport coefficients for every subsystem are related to the thermal conductivity of the subsystems, λ_i, by Fourier's law:

$$\lambda_i = -\frac{J_{q,\,i}}{\mathrm{d}T/\mathrm{d}z} = \frac{1}{T_i^2\,R^{interf}_{q,\,i}} \tag{23}$$

As interface thickness, we assume the tissue thickness relevant for the case (~0.01 mm). Since it is known that the surface has higher resistivity to transport than an homogeneous phase, we increase the value of the so-calculated interface transport coefficients by a factor of 10. The convective contribution to the heat transport coefficient, $R^{conv}_{q,\,i}$, is non-zero only in the arterial and venous subsystems, where there is convective blood flow. Due to its characteristics, the blood flow is considered to be laminar. Under this assumption, the Nusselt number is constant [30]:

$$\mathrm{Nu} = 3.66 \tag{24}$$

3.4 Heat and water recovery

As mentioned, heat and water are added to the air in the nasal cavity during inhalation and are subtracted from it during exhalation. In order to be able to compare the results of our calculations with those available in the work by Blix and Johnsen [6], we calculate these quantities with the same procedure as they used. The water that is added to the air stream upon inhalation, $M_{w,\,added}$, is calculated as the difference between the total amount of water that leaves the lungs during exhalation in the air stream and the total amount of water that enters the nostril during inhalation:

$$M_{w,\,added} = \int_{ex} \left(-F_{w,\,a}\right)_{z=L}\,dt - \int_{in} \left(F_{w,\,a}\right)_{z=0}\,dt \tag{25}$$

where L is the length of the nose, and $z = 0$ and $z = L$ refer respectively to the distal and the proximal extremity of the nose. Here, *ex* indicates the exhaling part of the breathing cycle ($\tau_{breath}/2 \le t \le \tau_{breath}$, where

τ_{breath} is the length of the breathing cycle), and *in* indicates the inhaling part ($0 \le t \le \tau_{breath}/2$). The water that is recovered during exhalation, $M_{w,recov}$, is the difference between the total amount of water that leaves the lungs during exhalation, and the total amount of water that leaves the nostril during exhalation:

$$M_{w,recov} = \int_{ex} (-F_{w,a})_{z=L}\, dt - \int_{ex} (-F_{w,a})_{z=0}\, dt \tag{26}$$

The recovery of water is given by the ratio between the water recovery upon exhalation and the water added upon inhalation.

The same procedure as in Ref. [6] is also used to calculate the heat added upon inhalation, Q_{added}. This quantity is calculated as the sum of the heat that is necessary to warm up the inhaled air to the body temperature and the heat that is necessary to evaporate the water that is added during inhalation:

$$Q_{added} = \int_{in} F_a\, c_{p,a} \left(T_{body} - T_{amb}\right) dt + M_{w,added}\, h_{lat} \tag{27}$$

where h_{lat} is the latent heat of vaporization or condensation of water, and its value is taken from Ref. [6]. The subscripts *amb* and *body* refer respectively to the thermodynamic variables describing the ambient air and the reindeer deep body conditions. The heat that is recovered during exhalation, Q_{recov}, is given by the sum of the sensible heat that is subtracted from the air during exhalation and the latent heat that is released by the condensing water:

$$Q_{recov} = \int_{ex} F_a\, c_{p,a} \left(T_{body} - T_{ex}\right) dt + M_{w,recov}\, h_{lat} \tag{28}$$

The recovery of heat can finally be defined as the ratio between the heat recovered upon exhalation and the heat added during inhalation.

A more comprehensive energy balance over all nasal subsystems can be used to determine how much of the reindeer energy is used during a breathing cycle, E_{body}:

$$E_{body} = \int_0^{\tau_{breath}} \left(-F_a\, h_a + F_b\, c_{p,b} \left(T_{body} - T_{ven}\right)\right)_{z=L} dt + \int_0^{\tau_{breath}} \left(\int_0^L \gamma_m\, J_m\, h_{w,m}\, dx \right) dt \tag{29}$$

3.5 Entropy production

According to non-equilibrium thermodynamics, the entropy production of a system, σ, is defined as the product sum of the conjugate fluxes, J_i, and forces, X_i, in the system [15]. For a cross section:

$$\sigma_A = \sum_i J_i\, X_i\, \gamma_i. \tag{30}$$

The mass and heat fluxes have been defined in Section 3.3 (eqs. (13), (14) and (22)) and the corresponding conjugate forces are represented by the terms on the left-hand side of the same equations. The integration of eq. (30) over the length of the nose and over the breathing cycle gives the total entropy produced in the nose during a breathing cycle, Σ_{irr}.

4 Solution procedure

With the given assumptions, all the mass balance equations equal 0, except the mass balances of the air (eqs. (1) and (2)). The energy balances provide a set of five partial differential equations (eqs. (7)–(11)), which

together with (eqs. (1) and (2)) give a total of seven partial differential equations. We transform the system of partial differential equations into a set of ordinary differential equations by discretizing in the spatial dimension. Further, we consider N_p discretization points in the z-dimension, and in each of these we approximate the first-order spatial derivatives by using a finite difference method (MatLab routines "dss020"). Thus, every partial differential equation is transformed into a set of N_p ordinary differential equations in time. In order to account for the boundary conditions, we replace the corresponding differential equations with the algebraic equations given by the boundary conditions (Section 4.1). Thus, we obtain a final set of ordinary differential and algebraic equations that we can solve with the solver "ode15s", in combination with a mass matrix.

The problem is inherently dynamic, meaning that the thermodynamic variables vary with time. However, in computations, after a sufficient amount of time, we should reach a pseudo-steady state, where the thermodynamic variables have the same values at corresponding times of consecutive breathing cycles. With a stable formulation of the problem, the results should not depend on the set of initial conditions that we choose. In practice, we stop the calculations when the difference between the temperatures at corresponding times of two consecutive breathing cycles is smaller than 0.01 K. In calculations, this condition is reached after about 400 breathing cycles.

4.1 Boundary conditions

Since we have first-order spatial derivatives of the temperatures and of the humid air water content, a set of seven appropriate boundary conditions is needed. A complete breathing cycle is composed of an inhalation part and of an exhalation part. The boundary conditions are different in different moments of the breathing cycle. During inhalation, the air that enters the distal extremity of the nose is at ambient conditions; therefore, its temperature, T_a, and water content, $\rho_{w,a}$, equal the corresponding ambient values, T_{amb} and $\rho_{w,a,amb}$. Moreover, we assume that the arterial blood temperature T_{art}, the mucus temperature T_m and the interstitial tissue temperature T_{it} at the base of the nose are equal to the deep body temperature of the reindeer, T_{body}. In addition, since at the distal extremity of the nose, arteries communicate directly with the veins, we assume that the temperature of the arterial blood equals the temperature of the vein blood at the distal extremity. The first six boundary conditions for inhalation are:

$$\rho_{w,a}(z=0) = \rho_{w,a,amb} \tag{31}$$

$$T_a(z=0) = T_{amb} \tag{32}$$

$$T_m(z=L) = T_{body} \tag{33}$$

$$T_{it}(z=L) = T_{body} \tag{34}$$

$$T_{art}(z=L) = T_{body} \tag{35}$$

$$T_{ven}(z=0) = T_{art}(z=0) \tag{36}$$

During exhalation, we assume that the air that enters the proximal extremity of the nose coming from the lungs is saturated air at deep body temperature. Therefore, during exhalation, the boundary conditions given by eqs. (31) and (32) are substituted by:

$$\rho_{w,a}(z=L) = \rho_{w,a,body} \tag{37}$$

$$T_a(z=L) = T_{body} \tag{38}$$

The last boundary condition involves the dry air flow at the distal extremity of the nose, which is set to be a known function of time. Experimental data on the dry air flow are necessary to determine this function. We use the value of the respiratory minute volume, $V_{\min}$, from Ref. [6] and assume that the air flow is a sinusoidal function of time similar to previous work [32]. A resting phase between inhalation and exhalation is not considered, and the dry air flow at the distal extremity of the nose is described as:

$$F_{dry} = F_{dry,\,\max} \sin\left(\frac{2\pi}{\tau_{breath}} t\right) \tag{39}$$

where $F_{dry,\,\max}$ is the maximum value of the dry air flow during the breathing cycle. We calculate $F_{dry,\,\max}$ from the value of respiratory minute volume.

4.2 Relevant data

In order to perform calculations, we must rely on experimental data. Table 1 summarizes some of the relevant data for calculations. The heat capacity, the density and the thermal conductivity of the blood are assumed to be constant. We also assume that the same values can be used to describe the interstitial tissues, and that the mucus can be described by the properties of water. No experimental data are available on blood flow in the reindeer nose. However, data exist on carotid artery blood flow to the head (~4.8 g/s [33]). We assume that the fraction of carotid artery blood flow that goes to the nose is of a magnitude that gives a blood velocity in the nasal vessels that is within the typical range of blood velocities in small vessels (i. e. in the order of 1–10 mm/s [34]). The geometry of the reindeer nose has been accurately determined by the anatomical study in Ref. [10], to which we refer for the geometrical data of every subsystem.

Table 1: Data relevant for calculations. Here, φ_{amb} is the relative humidity of the ambient air, p_a is the ambient pressure, $f_a = 1/\tau_{breath}$ is the respiration frequency, and $M_{reindeer}$ is the mass of the reindeer. The ambient air relative humidity is used to calculate the density of water in the ambient air, $\rho_{w,a,amb}$.

	Value	Unit
φ_{amb}	90	%
p_a	1.0	bar
$V_{\min}$	0.1	l/min/kg [6]
f_a	10	$\min^{-1}$ [6]
$M_{reindeer}$	54	kg [10]
T_{body}	312	K [6]
$c_{p,b}$	4.2	kJ/kg/K
ρ_b	1.0	kg/dm^3
k_b	0.5	J/m/s/K
F_b	0.2	g/s
$c_{p,m}$	4.2	kJ/kg/K
ρ_m	1.0	kg/dm^3
k_m	0.6	J/m/s/K

The large variation in the geometry of the nasal cavity is illustrated in Figure 3. Similar data are available for the other subsystems. The example animal was a sub-adult female (body mass ~54 kg), thus being somewhat smaller than the average adult animal.

5 Results and discussion

5.1 Air-flow velocity

A direct consequence of the large variation in the cross-sectional area of the nasal cavity of the reindeer is that the velocity profile of the air varies accordingly. Figure 4 depicts the air-velocity profile during

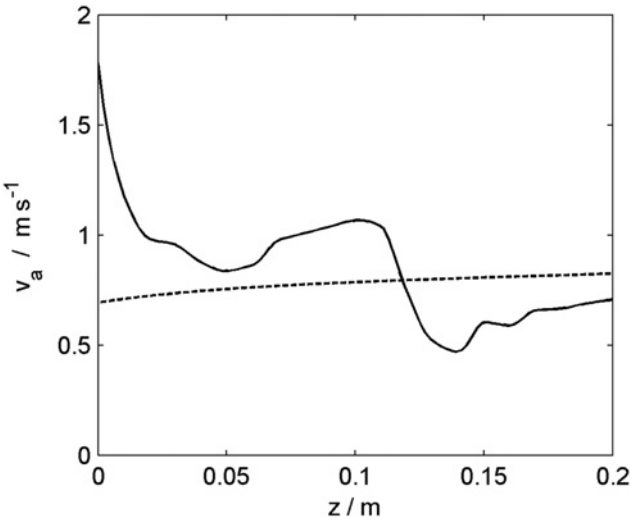

Figure 4: Velocity of the inhaled air along the nasal cavity, at $\left(t = \frac{1}{4}\tau_{breath}\right)$ for System A (solid line) and System B (dashed line). Calculations are carried out at $T_{amb} = 273$ K.

inhalation, when the air flow is maximum $\left(t = \frac{1}{4}\tau_{breath}\right)$. The solid line represents the velocity of the air across System A. Comparison with Figure 3 shows the strong correlation between the velocity of the air and the cross-sectional area of the nasal cavity. Indeed, the air slows down where the cross-sectional area is larger, while it accelerates where the area of the cross section is smaller. Since the cross section of the air cavity is constant in System B, the variation of the air velocity occurs only due to the change in the air density (dashed line in Figure 4). The increase in the air velocity takes place due to the warming of the air flow, as it proceeds in the nasal cavity, from the distal to the proximal extremity. Similar considerations apply to the velocity of the blood in arteries and veins (results are not reported). Since the blood density has been assumed to be constant, the blood velocity is constant throughout the system for System B.

5.2 Temperature

Since the transfer processes in the reindeer nose during respiration are dynamic, we can either investigate the instantaneous temperature of a subsystem or define an average temperature over the breathing cycle. Figure 5 depicts the instantaneous temperature profiles in the five subsystems at four different times of the breathing cycle. Figure 5(a) shows the temperature profiles when the breathing cycle begins ($t = 0$). At this instant, the air flow is 0, and inhalation is about to start. The air in the nasal cavity at this time (black lines) is almost at thermal equilibrium with the mucus layer that covers the cavity walls (cyan lines). Figure 5(b) shows the temperatures at $t = \frac{1}{4}\tau_{breath}$, when the inhaled air flow is at its maximum. Since cold air is inhaled from the ambient, its temperature along the nose is lower than that of the mucus layer, and heat is transferred from the mucus to the air. From this moment on, the velocity of the air decreases to become 0 at $t = \frac{1}{2}\tau_{breath}$ (Figure 5(c)), when exhalation begins. Similarly to the temperature at $t = 0$, the temperatures of the air and the mucus are then almost the same. Figure 5(d) presents the profiles for the instant of maximum air flux during exhalation $\left(t = \frac{3}{4}\tau_{breath}\right)$. Here, the air flow is negative, and the air flows from right to left. Since the air comes from the lungs, the air temperature is higher than the temperature of the mucus, and heat is transferred from the air to the wet walls of the nose. The solid lines depict the results obtained for System A, while the dashed lines show the results for System B.

The temperature of the air at the distal extremity of the nose ($z = 0$) during inhalation is equal to the ambient temperature. However, during exhalation, the air temperature at this location is higher than the one of the ambient, meaning that not all the heat that was provided to the air stream upon inhalation is recovered.

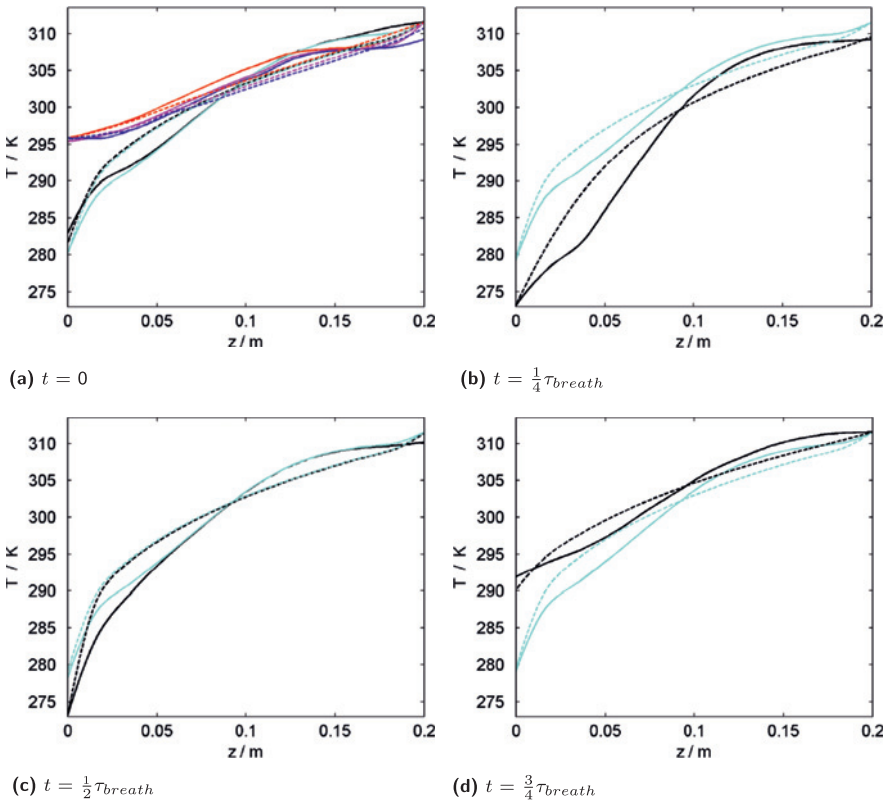

(a) $t = 0$ (b) $t = \frac{1}{4}\tau_{breath}$

(c) $t = \frac{1}{2}\tau_{breath}$ (d) $t = \frac{3}{4}\tau_{breath}$

Figure 5: The instantaneous temperatures in the subsystems at four different times of the breathing cycle, for System A (solid line) and System B (dashed line). The coloring of the lines is as following: black for the temperature of the air, cyan for mucus, magenta for interstitial tissue, red for arterial blood and blue for venous blood. Curves for interstitial tissue, arterial blood and venous blood were left out from panels (b) through (d) for the sake of clarity. Calculations are carried out at $T_{amb} = 273$ K.

Except for the air, the mucus layer is the subsystem which has the largest variation in temperature during a breathing cycle. This is mainly due to condensation and evaporation of water. During inhalation, the mucus layer is cooled down as water evaporates from it to humidify the air stream. Since the evaporation rate is largest near the distal extremity of the nose, the mucus layer at this location has the largest temperature drop during inhalation (~1.9 K). During exhalation, water condenses from the air stream to the mucus layer that has been cooled down during inhalation. This increases the temperature of the mucus, as it receives the latent heat released during condensation of water.

The temperature profiles of the interstitial tissues and of the blood flowing in vessels do not change considerably over the breathing cycle (<0.5 K). We have therefore reported the temperature profiles of these subsystems only in Figure 5(a). The reason for the moderate change in these temperatures is that the interstitial tissues have a large total heat capacity. Since the blood interacts mainly with the interstitial tissues (see Figure 2), the temperature change of the blood will also be delayed. Moreover, the difference between the blood temperature in arteries and veins (red and blue lines) and the interstitial tissue temperature (magenta lines) is very small, indicating that the heat exchange between these subsystems is very fast. This is in agreement with the findings in several other works [35, 36], where small vessels such as arterioles and venules are found to be almost in thermal equilibrium with the tissues they run through. A comparison between the results obtained with System A (solid lines) and those obtained with System B (dashed lines) shows that the exhaled air temperature and the temperature of the air entering the lungs are very similar for the two cases. Since the total contact areas between the subsystems are the same for System A and System B, we expect no major differences in the total amount

of heat exchanged between the subsystems. The maximum difference between the exhaled air temperature obtained with the two different systems at the same times of the breathing cycle is ~2 K. The different geometrical configuration of the systems has mainly an influence on the temperature profiles.

Figure 5 shows that the temperatures of all five subsystems in the distal part of the nose are on average lower in System A than in System B, while the opposite happens in the other part of the nose.

Since many assumptions have been made in developing the model of the reindeer nose, it is important to compare to experimental data to assess the accuracy of the model. Johnsen et al. [22] reported the temperature of the nasal mucosa at different locations inside the nose of a breathing reindeer at different ambient air temperatures. Figure 6 compares the experimental measurements with the results from the model of the reindeer nose (System A) under the same ambient conditions. Since the experimental temperatures are available just as average values over the breathing cycle, we define the average temperature as the integral in time of the temperature over a breathing cycle divided by the total time of the breathing cycle. Figure 6 shows that some discrepancies exist between the two profiles, and temperatures from the model are in general lower than those from the experimental results. Nonetheless, the experimental temperature trend is predicted reasonably well by the model. Some expected differences are caused by the fact that the model parameters are based on a different animal than the one studied by Johnsen et al. [22]. However, several other factors concur to the differences between the theoretical and the experimental profiles. First of all, in the modeling of the vascular system, we are accounting only for the larger blood vessels, such as arteries and veins, while smaller vessels (e. g. capillaries) are not considered. A previous study [37] showed that blood vessels with a diameter smaller than 25 μm have a fundamental role in the nasal microcirculation. Moreover, since no experimental data for the total blood flow in the reindeer nose are available, we have assumed a blood flow which gives blood velocities within realistic physiological limits for reindeer. Accounting for the smaller vessels would therefore result in a larger blood flow through the nose, with the same blood velocity. Since the blood flow is responsible for providing heat to the nose, a higher blood flow would cause a higher average temperature of all subsystems. An additional explanation of the deviation from experimental data can be attributed to the fact that the tissues next to the nasal orifice are most likely perfused by independent blood vessels [22] in order to prevent the tissues from freezing under very low ambient temperature. The experimental data in Figure 6 support this explanation, since the temperature of the mucosa next to the distal extremity of the nose is higher than the temperature of the tissue in the central section of the nose.

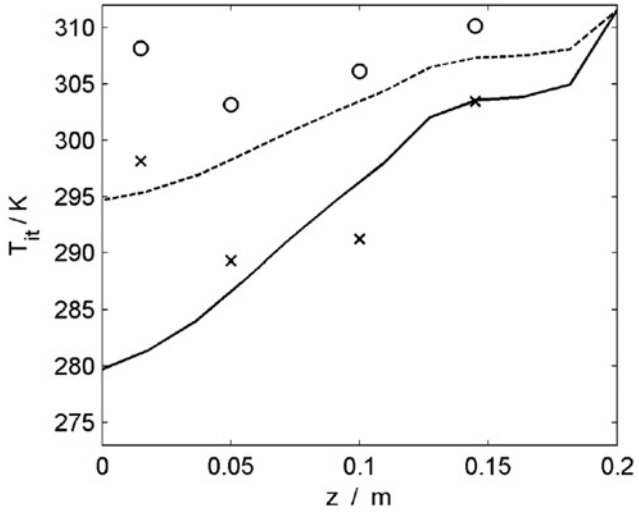

Figure 6: Comparison between the model prediction for the interstitial tissue averaged temperature (lines) and experimental data [22] (symbols) along the length of the nasal cavity, at $T_{amb} = 243$ K (solid line and crosses), and at $T_{amb} = 273$ K (dashed line and circles).

This phenomenon cannot be explained without introducing independent vessels perfusing the distal part of the nose. In the present work, we do not account for such vessels. Nonetheless, Figure 6 shows that the

model presented in this work is capable of capturing the trend in the experimental data well. A model with increased complexity is necessary to account for the rise in temperature at the distal extremity of the nose.

Experimental data on the average exhaled air temperature are also available [22]. Table 2 compares the experimental measurements with the results from the model. The average temperature is here calculated as the integral in time of the product of the exhaled air temperature and the exhaled air mass flow divided by the integral of the exhaled air mass flow. The computed temperatures of the exhaled air are lower than those from the experiments. Also here, the reason for this is that the rise in temperature of the interstitial tissue in proximity of the nasal orifice is not accounted for in the present model.

Table 2: Comparison between the computed averaged temperature of the exhaled air obtained with System A, $T_{ex,\,comp}$, and the exhaled air temperature from experimental measurements, $T_{ex,\,exp}$ [22].

T_{amb} (K)	$T_{ex,\,comp}$ (K)	$T_{ex,\,exp}$ (K)
243	278	287
273	291	303

5.3 Water content of the air

Figure 7 depicts the water mass fraction in the air stream during inhalation, when the air flow is at its maximum $\left(t = \frac{1}{4}\tau_{breath}\right)$. The solid line shows the results for System A, while the dashed line represents System B. The water mass fraction in the air at the distal extremity of the nose equals the ambient water mass fraction, since air is inhaled. The difference in the water content of the inhaled air between System A and System B at the proximal extremity of the nose (where the air is about to enter the trachea) is almost negligible. As we have seen in Figure 5, the different geometrical configuration of the systems influences mainly the temperature profiles. Figure 7 shows that the water content of the air in the part of the nose closer to the distal extremity is on average lower in System A than in System B, while the opposite happens in the other part of the nose. An analogous behavior was observed for the temperature profiles. During exhalation (not reported here), the air that comes from the lungs enters the nose at the proximal extremity of the nose ($z = L$) as saturated air at body temperature. During exhalation, the water content of the air that leaves the nose is higher than the one of the inhaled air, meaning that not all the water that is added during inhalation is recovered upon exhalation.

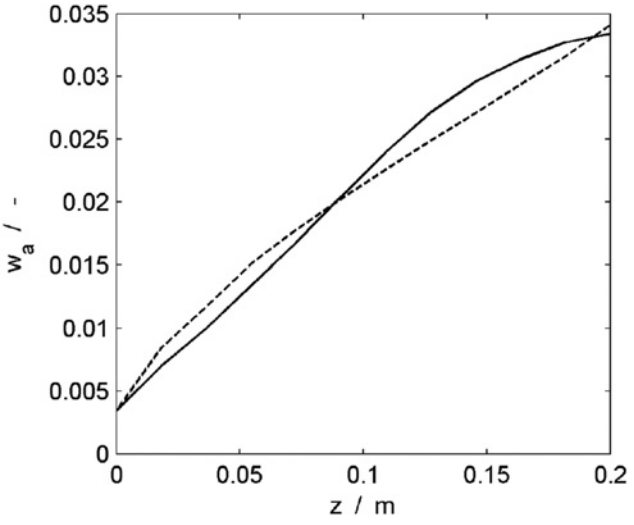

Figure 7: Water mass fraction in the inhaled air, at $t = \frac{1}{4}\tau_{breath}$ for System A (solid line) and System B (dashed line). Calculations are carried out at $T_{amb} = 273$ K.

5.4 Heat and water recovery

Heat and water are added to the air in the nasal cavity during inhalation and are recovered from the air during exhalation. Table 3 reports the percentage of the added heat and water that is recovered with System A and System B. Since the overall surface through which heat and mass are exchanged is the same for the two systems, the results in Table 3 show no major differences between the heat and water recovered with the two different structures. However, the more complicated geometrical structure of the reindeer nose allows for a slightly better recovery of heat and water at lower temperatures, while it is less efficient at higher temperatures. The recovery of both heat and water increases with decreasing temperature, as the temperature (and therefore the water content) of the exhaled air is lower. Moreover, at lower ambient temperatures, the amount of heat and water that is provided to the air stream during inhalation increases. For both System A and System B, the high recovery of water is correlated to the low temperature of the exhaled air. At this ambient temperature, the absolute humidity of the saturated air is also very low, making the percentage of recovered water very high. In Section 5.2, we saw that the calculated temperature of the exhaled air is lower than the one measured experimentally. Higher exhaled air temperatures would cause a reduction in the fraction of water that is recovered upon exhalation. For instance at $T_{amb} = 243\,K$, with the temperature of the exhaled air equal to 287 K (see Table 2), only 71% of water would be recovered.

Calculations of water and heat lost upon exhalation for reindeer are available in the work by Blix and Johnsen [6]. Table 4 compares these calculations with the results from our model. In Ref. [6], the respiratory minute volume was not constant for varying ambient temperature. Therefore, in this set of calculations we consider the respiratory minute volume to be a function of the ambient temperature in order to be able to compare the experimental results and the model. Table 4 shows that the heat and water losses from the model are systematically lower than those reported in Ref. [6]. Again, this discrepancy can be attributed to the temperature of the exhaled air, which is much lower in the model compared to the experimental results. For instance, with an exhaled air temperature of 287 K (see Table 2) at $T_{amb} = 243\,K$, the heat and water losses resulting from our calculations would be respectively 426 J/min and 56 mg/min, which are the values that are satisfactory in agreement with the results from Ref. [6].

Table 3: Heat and water recovery for System A and System B, at different ambient temperatures.

T_{amb} (K)	Heat recovery		Water recovery	
	System A (%)	System B (%)	System A (%)	System B (%)
243	88.3	88.2	99.5	99.4
253	86.5	86.6	98.3	98.2
263	81.7	82.6	96.2	96.5
273	76.4	77.4	92.3	92.5

Table 4: Comparison between the heat and water lost in 1 min for System A and data from [6], at different ambient temperatures and respiratory minute volumes.

T_{amb} (K)	V_{min} (l/min/kg)	Heat lost (J/min)		Water lost (mg/min)	
		System A	Ref. [6]	System A	Ref. [6]
243	0.10	263	484	1.4	54
253	0.15	345	684	5.8	108
263	0.20	402	972	18.5	206
273	0.25	428	1,361	40.3	394

5.5 Entropy production and total energy consumption

Even though there are no major differences in the heat and water recovery between System A and System B, the entropy production of the two configurations is very different. Figure 8 depicts the local entropy production that takes place during a breathing cycle, in System A (solid line) and in System B (dashed line). Most of the entropy is produced during inhalation (not shown). When cold air enters the distal extremity of the nose, there are large thermodynamic driving forces for heat and mass transfer between the air stream and the mucus layer. This causes the local entropy production to be very high at this location, as depicted in Figure 8. However, as we have seen in Figure 3 the cross-sectional perimeter in System A is smaller at this location than in the central part of the nasal cavity, where driving forces and fluxes become smaller. According to eq. (30), this causes the local entropy production of each cross section to be more uniform in System A than the entropy production of System B, where the entropy production at this location is almost one order of magnitude larger than in the remaining part of the system.

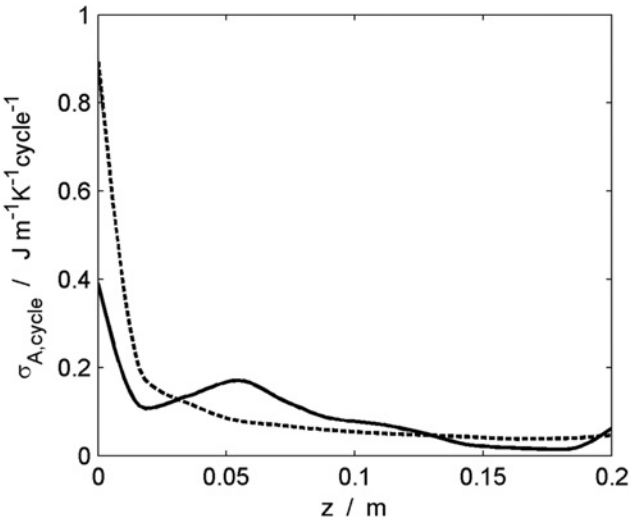

Figure 8: Comparison between the cross-section entropy production of a breathing cycle, for System A (solid line) and System B (dashed line). Calculations are carried out at $T_{amb} = 243$ K.

In recent years, a hypothesis was formulated, stating that a system with minimum total entropy production (or dissipated energy) is a system with uniform distribution of entropy production over the system's extension in space and time [14, 16]. A previous study of the human lungs showed that during respiration, the lungs are characterized by a uniform local entropy production in the bronchial tree [38], suggesting that the principle of uniform entropy production might also guide the evolution of biological systems. In agreement with this hypothesis, our results show that the structure of the reindeer nose could have evolved to give a more uniform entropy production, compared to a simpler geometry, to enhance the energy efficiency. This is further supported by Table 5, which reports the total entropy production per cycle, obtained through a spatial

Table 5: Total entropy production during a breathing cycle in System A and System B at different ambient temperatures.

T_{amb} (K)	Σ_{irr} (J/K/cycle)		Reduction in System A
	System A	System B	w.r.t. System B (%)
243	0.0162	0.0195	−20
253	0.0120	0.0139	−16
263	0.0086	0.0096	−12
273	0.0056	0.0061	−9

integration of the local entropy production, $\sigma_{A,cycle}$. For all the investigated ambient temperatures in Table 5, the total entropy production is always lower in System A than in System B.

The reduction in the total entropy production is largest at low ambient temperatures. With an ambient temperature of 243 K, System A produces 20 % less entropy than System B. The geometry of the reindeer nose therefore appears to be designed to be extra energy efficient at very low ambient temperatures. This suggests that natural selection has favored designs that give uniform entropy production when energy efficiency is an issue, presumably because this is beneficial for the survival of the animal.

Indeed, less entropy production is directly related to a lower consumption of the animal's energy during the respiration process. In Section 5.4, the heat and water recovered from the exhaled air were the only parameters considered as a measure of the efficiency of respiration, and they were calculated with the same approximated method used in Ref. [6] in order to make the results comparable. A more comprehensive energy balance over all nasal subsystems (eq. (29)) shows that System A uses less of the total available energy of the animal during a respiration cycle. At the lowest temperature (243 K), System A requires ~0.9 J/cycle of the body energy of the animal less than System B (Table 6). Since the consumed energy needs to be supplied to the animal in the form of food, a lower consumption of energy gives the animal a better chance of surviving with scarce food/energy conditions.

Table 6: Body energy consumption during a breathing cycle in System A and System B, at different ambient temperatures.

T_{amb} (K)	E_{body} (J/cycle)		Reduction in System A
	System A	System B	w.r.t. System B (%)
243	26.3	27.1	−3.3
253	20.5	21.0	−2.3
263	17.6	17.9	−1.7
273	11.6	11.7	−1.2

The geometrical design of the reindeer nose, or of other animals that must survive in the harsh arctic climate, may serve as an inspiration to design the geometry of more energy-efficient equipment in industry or in the society.

6 Conclusion

We have presented a detailed dynamic model to describe the transport of heat and mass that takes place inside the nose of an arctic reindeer during respiration. The dynamic model correctly captures the trend in published experimental data for the temperature, heat and water recovery in the reindeer nose during respiration. As a reference case, we modeled a nose with a simple cylindrical-like geometry, where the total volume and contact area were the same as in the reindeer nose. We found that the complicated geometry of the reindeer nose did not offer significant advantages compared to the reference case for conserving the heat and the water in the air. This was expected, since the total contact area and volume were the same. However, the complicated geometry of the reindeer nose had a large influence on the temperature profiles of the air flowing through the nose during respiration.

For all investigated cases, the total entropy production of a breathing cycle was smaller for the reindeer nose than for the reference case. The same trend could be observed for the total energy consumption of the animal. This means that the complex geometry of the reindeer nose increases its energy efficiency. The reduction in the total entropy production was largest at the lowest ambient temperatures. At an ambient temperature of 243 K, the reindeer nose produced 20 % less entropy than the reference case. The geometry

of the reindeer nose therefore appears to be more important at lower ambient temperatures when energy efficiency is more critical for the survival of the animal. In the literature, an hypothesis has been proposed, stating that the most energy efficient design of a system is characterized by equipartition of the entropy production. In agreement with this hypothesis, we found that the local entropy production during a breathing cycle was significantly more uniform for the reindeer nose than for the reference case. This suggests that natural selection may have favored constructions with uniform entropy production when energy efficiency is an issue.

The geometry of the reindeer nose increases the energy efficiency of the respiration cycle, and thereby reduces the energy requirements of reindeer in the harsh arctic climate. The geometry of the reindeer nose can thus serve as inspiration for designing energy-efficient equipment where simultaneous heat and mass transfer occurs, such as air ventilation systems in buildings.

Acknowledgements: The project is funded by VISTA – a basic research program in collaboration between The Norwegian Academy of Science and Letters, and Statoil – and by the Tromsø Research Foundation.

References

[1] K. J. Nilssen, H. K. Johnsen, A. Rognmo and A. S. Blix, Heart rate and energy expenditure in resting and running svalbard and norwegian reindeer, *Am. J. Physiol. Regul. Integr. Comp. Physiol.* **246** (1984), no. 6, R963–R967.
[2] I. Moote, The thermal insulation of caribou pelts, *Text. Res. J.* **25** (1955), no. 10, 832–837.
[3] J. Timisjärvi, M. Nieminen and A.-L. Sippola, The structure and insulation properties of the reindeer fur, *Comp. Biochem. Physiol. A: Physiol.* **79** (1984), no. 4, 601–609.
[4] H. Johnsen, A. Rognmo, K. Nilssen and A. Blix, Seasonal changes in the relative importance of different avenues of heat loss in resting and running reindeer, *Acta Physiol. Scand.* **123** (1985), no. 1, 73–79.
[5] L. P. Folkow and J. B. Mercer, Partition of heat loss in resting and exercising winter-and summer-insulated reindeer, *Am. J. Physiol. Regul. Integr. Comp. Physiol.* **251** (1986), no. 1, R32–R40.
[6] A. S. Blix and H. K. Johnsen, Aspects of nasal heat exchange in resting reindeer, *J. Physiol.* **340** (1983), no. 1, 445–454.
[7] K. Schmidt-Nielsen, F. R. Hainsworth and D. E. Murrish, Counter-current heat exchange in the respiratory passages: effect on water and heat balance, *Respir. Physiol.* **9** (1970), no. 2, 263–276.
[8] A. Blix, H. Johnsen and J. Mercer, On nasal heat-exchange and the structural basis for its regulation in reindeer, *J. Physiol.-London* **343** (1983), 108–109.
[9] H. K. Johnsen, *Nasal heat exchange: an experimental study of effector mechanisms associated with respiratory heat loss in Norwegian reindeer (Rangifer tarandus tarandus)*, Ph.D. thesis, 1988.
[10] I. L. Casado Barroso, The ontogeny of nasal heat exchange structures in arctic artiodactyles (2014).
[11] M. C. Wika, J. O. Krog and R. Hol, Vascular structure in the nasal cavity of reindeer, in: *The Peripheral Circulation: Proceedings of the International Symposium on the Peripheral Circulation* (Newport, Sydney, September 5–6, 1983), vol. **630**, p. 161, Excerpta Medica, 1984.
[12] S. Kjelstrup, M.-O. Coppens, J. Pharoah and P. Pfeifer, Nature-inspired energy-and material-efficient design of a polymer electrolyte membrane fuel cell, *Energy Fuels* **24** (2010), no. 9, 5097–5108.
[13] A. Zlotorowicz, K. Jayasayee, P. Dahl, M. Thomassen and S. Kjelstrup, Tailored porosities of the cathode layer for improved polymer electrolyte fuel cell performance, *J. Power Sources* **287** (2015), 472–477.
[14] E. Johannessen and S. Kjelstrup, A highway in state space for reactors with minimum entropy production, *Chem. Eng. Sci.* **60** (2005), no. 12, 3347–3361.
[15] S. Kjelstrup and D. Bedeaux, *Non-equilibrium Thermodynamics of Heterogeneous Systems*, Singapore: World Scientific, 2008.
[16] Ø. Wilhelmsen, E. Johannessen and S. Kjelstrup, Energy efficient reactor design simplified by second law analysis, *Int. J. Hydrogen Energy* **35** (2011), 13219–13231.
[17] D. Elad, M. Wolf and T. Keck, Air-conditioning in the human nasal cavity, *Respir. Physiol. Neurobiol.* **163** (2008), no. 1, 121–127.
[18] S. Naftali, R. Schroter, R. Shiner and D. Elad, Transport phenomena in the human nasal cavity: a computational model, *Ann. Biomed. Eng.* **26** (1998), no. 5, 831–839.
[19] S. Naftali, M. Rosenfeld, M. Wolf and D. Elad, The air-conditioning capacity of the human nose, *Ann. Biomed. Eng.* **33** (2005), no. 4, 545–553.

[20] F. Castro, T. Parra, C. Quispe and P. Castro, Numerical simulation of the performance of a human nasal cavity, *Engin. Comput.* **28** (2011), no. 6, 638–653.
[21] J. Collins, T. Pilkington and K. Schmidt-Nielsen, A model of respiratory heat transfer in a small mammal, *Biophys. J.* **11** (1971), no. 11, 886–914.
[22] H. K. Johnsen, A. S. Blix, L. Jorgensen and J. B. Mercer, Vascular basis for regulation of nasal heat exchange in reindeer, *Am. J. Physiol. Regul. Integr. Comp. Physiol.* **249** (1985), no. 5, R617–R623.
[23] H. A. Jakobsen, Chemical reactor modeling, in: *Multiphase Reactive Flows*, Springer-Verlag, Berlin, Germany (2008).
[24] Ø. Wilhelmsen, D. Bedeaux and S. Kjelstrup, Heat and mass transfer through interfaces of nanosized bubbles/droplets: the influence of interface curvature, *Phys. Chem. Chem. Phys.* **16** (2014), 10573.
[25] Ø. Wilhelmsen, T. T. Trinh, S. Kjelstrup, T. S. van Erp and D. Bedeaux, Heat and mass transfer across interfaces in complex nanogeometries, *Phys. Rev. Lett.* **114** (2015), no. Feb, 065901.
[26] L. Onsager, Reciprocal relations in irreversible processes. I., *Phys. Rev.* **37** (1931), no. Feb, 405–426.
[27] L. Onsager, Reciprocal relations in irreversible processes. II., *Phys. Rev.* **38** (1931), no. Dec, 2265–2279.
[28] Ø. Wilhelmsen, T. T. Trinh, A. Lervik, V. K. Badam, S. Kjelstrup and D. Bedeaux, Coherent description of transport across the water interface: From nanodroplets to climate models, *Phys. Rev. E* **93** (2016), no. Mar, 032801.
[29] J. Wen, K. Inthavong, Z. Tian, J. Tu, C. Xue and C. Li, Airflow patterns in both sides of a realistic human nasal cavity for laminar and turbulent conditions, in: *16th Australasian Fluid Mechanics Conference (AFMC)*, School of Engineering, The University of Queensland (2007), 68–74.
[30] Y. A. Cengel and J. Hernán Pérez, *Heat Transfer: A Practical Approach*, McGraw-Hill, México, 2004.
[31] P. Zamankhan, G. Ahmadi, Z. Wang, P. K. Hopke, Y.-S. Cheng, W. C. Su, et al., Airflow and deposition of nano-particles in a human nasal cavity, *Aerosol Sci. Technol.* **40** (2006), no. 6, 463–476.
[32] S. Ishikawa, T. Nakayama, M. Watanabe and T. Matsuzawa, Visualization of flow resistance in physiological nasal respiration: analysis of velocity and vorticities using numerical simulation, *Arch. Otolaryngol. Head Neck Surg.* **132** (2006), no. 11, 1203–1209.
[33] A. S. Blix, L. Walløe and L. P. Folkow, Regulation of brain temperature in winter-acclimatized reindeer under heat stress, *J. Exp. Biol.* **214** (2011), no. 22, 3850–3856.
[34] K. Ivanov, M. Kalinina and Y. Levkovich, Blood flow velocity in capillaries of brain and muscles and its physiological significance, *Microvasc. Res.* **22** (1981), no. 2, 143–155.
[35] J. Chato, Heat transfer to blood vessels, *J. Biomech. Eng.* **102** (1980), no. 2, 110–118.
[36] M. M. Chen and K. R. Holmes, Microvascular contributions in tissue heat transfer, *Ann. N. Y. Acad. Sci.* **335** (1980), no. 1, 137–150.
[37] C. Ince, A.-M. van Kuijen, D. M. Milstein, K. Yürük, L. P. Folkow, W. J. Fokkens, et al., Why Rudolph's nose is red: observational study, *BMJ* **345** (2012), e8311.
[38] S. Gheorghiu, S. Kjelstrup, P. Pfeifer and M.-O. Coppens, Is the lung an optimal gas exchanger?, in: *Fractals in Biology and Medicine*, Springer (2005), 31–42.